Faculty and Researchers   Faculty and Researchers' Publications

2008-10-02

Real-time terahertz imaging of nonmetallic objects for security screening and anti-counterfeiting applications

Behnken, Barry N.; Karunasiri, Gamani

SPIE

Behnken, Barry N., and Gamani Karunasiri. "Real-time terahertz imaging of nonmetallic objects for security screening and anti-counterfeiting applications." Millimetre Wave and Terahertz Sensors and Technology. Vol. 7117. International Society for Optics and Photonics, 2008.
http://hdl.handle.net/10945/60324

PROCEEDINGS OF SPIE

Real-time terahertz imaging of nonmetallic objects for security screening and anti-counterfeiting applications

Barry N. Behnken, Gamani Karunasiri

Real-time terahertz imaging of nonmetallic objects for security screening and anti-counterfeiting applications

Barry N. Behnken[*] and Gamani Karunasiri
Department of Physics, Naval Postgraduate School, 833 Dyer Rd, Monterey, CA, USA 93943

ABSTRACT

We report the use of a 160×120 pixel microbolometer camera, under illumination by a milliwatt-scale 3.6 THz quantum cascade laser, for real-time imaging of materials which are exclusively nonmetallic in character. By minimizing diffraction effects suffered by the camera system and operating the laser at bias currents approaching saturation values, an imaging scheme was developed in which overlapping samples of nonmetallic materials can be imaged with high fidelity and long persistence times. Furthermore, an examination of various security features embedded within domestic and foreign currency notes suggests that this imaging scheme could serve a future role in detection of assorted counterfeiting practices.

Keywords: THz, terahertz, microbolometer, uncooled, quantum cascade laser, real-time, imaging, detection, security, counterfeiting, nonmetallic.

1. INTRODUCTION

A recent increase in homeland security concerns has precipitated a simultaneous demand for new imaging technologies. Of particular interest is the development of imaging systems that can quickly and efficiently detect concealed objects without posing health risks to humans. Owing to its unique spectral characteristics, radiation in the 0.3-10 terahertz (THz) spectral range has drawn recent attention as a new and potentially powerful medium for next-generation imaging technology.[1-14] Equipped with an appropriate illuminating source and sensor, terahertz imaging systems are capable of stand-off imaging of concealed objects and of human body tissue—particularly cancerous growths, which can elude x-ray based imaging detection.[5-7] Such detection agility is possible because terahertz wavelengths are short enough to provide sub-millimeter resolution capability, yet are also long enough to penetrate most non-metallic materials.[7] At the same time, terahertz radiation is strongly reflected by nearly all metallic substances—providing a unique opportunity for high-contrast imaging of metal objects concealed in common materials such as fabric, paper, or plastic. This capability makes terahertz imaging a useful technology for identification of many dangerous or prohibited objects. Furthermore, the non-ionizing nature of terahertz radiation allows it to be used directly with humans without incurring the health hazards associated with other imaging technologies. For these reasons, terahertz technology holds promise as a multi-fold solution to what is perhaps the most pernicious homeland security issue today: fast, safe, and effective screening of passengers and their belongings at mass-transit accumulation points, as well as stand-off identification of hazardous materials or weapons.

Currently, most THz imaging systems are based on either antenna-coupled semiconductor detectors or cryogenically-cooled bolometers operating in the scan mode.[1-4] While successful, these techniques are disadvantaged by a lack of portability, slow response, the need for cryogenic cooling, and/or high expense. A relatively new method of terahertz imaging invokes a different approach: the use of microbolometer cameras. Because this technology is based upon temperature-driven changes in pixel resistivity that are produced by the absorption of incident photons (rather than electron-hole generation/recombination, as is used in most semiconductor-based photodetectors), the devices are not susceptible to thermal excitation and can be routinely operated at room temperature. Furthermore, the relatively short thermal time constant (10 ms) of the microbolometer focal plane array (FPA) allows real-time imaging at television frame rates (30 Hz).

---

[*] bnbehnke@nps.edu; phone (831) 224-7630; http://www.nps.edu

Recent progress in the use of thermal detectors for terahertz imaging has soundly confirmed that microbolometer pixel membranes remain sensitive to radiation well outside the design (8-12 μm) wavelength range.[10-14] Despite the fact that mid-terahertz photon energies are a full order of magnitude lower than those of the infrared, microbolometer cameras have been successfully used to produce high-contrast images of metallic objects concealed by a wide range of nonmetallic materials. Such contrast is achieved by virtue of the dramatically different manner in which metals and nonmetals respond to terahertz illumination. Owing to the relatively high transparency of most non-metals to terahertz radiation, however, contrast between such materials has historically been more difficult to achieve. In this paper, we report the use of a 160×120 pixel microbolometer camera, under illumination by a milliwatt-scale 3.6-THz quantum cascade laser (QCL), for real-time imaging of both metallic and nonmetallic materials. By minimizing diffraction effects suffered by the camera system and operating the QCL at bias currents approaching saturation values, an imaging scheme was developed in which overlapping samples of nonmetallic materials can be imaged with high fidelity and long persistence times. Furthermore, an examination of various security features embedded within domestic and foreign currency notes suggests that this imaging scheme could serve a future role as a detection mechanism against assorted counterfeiting practices. Such results confirm the promise of this technology for future use in various homeland security applications.

2. IMAGING SYSTEM

2.1 Microbolometer Sensor

The microbolometer camera used in this research (IR-160, Infrared Solutions) employs a 160×120 pixel FPA which is sensitive to radiation falling within the 8-14 μm wavelength range. The camera has a dynamic range of 66 dB, a nominal noise equivalent power (NEP) of 35 pW, and, when operated in the infrared regime with f/0.8 optics, and an NETD of less than 100 mK.[13-14] The pixels are constructed, using conventional MEMS techniques, of a composite film of vanadium oxide (VO_x) and silicon nitride (Si_3N_4) with dimensions of 50×50 μm^2.[15] For use under terahertz illumination, the original germanium-based camera optics were replaced with a 1-inch diameter, 20-mm focal length bi-convex lens made of Tsurupica (PPL-1"-20 mm-BC, Microtech Instruments). Tsurupica, formerly known by the trade name Picarin, exhibits a transmissivity at 3.6 THz of roughly $T_l= 0.60$.

With over 35% of total radiative power of the 300 K blackbody spectrum lying within the 8-14 μm range, the device has a relatively low noise equivalent temperature difference (NETD) at room temperature (less than 100 mK when used with f/0.8 optics) which allows for generation of high-quality infrared images under passive operation. These radiometric conditions, which allow for outstanding performance in the infrared regime, act as technical obstacles to a microbolometer detector operating in the terahertz regime. As graphically depicted in Fig. 1, total radiative power emitted by a 300 K blackbody in the 1-5 THz spectral range is only one-twentieth of that associated with the design infrared band. Due to this stark disparity in available illumination power—combined with the well-established premise that IR-tuned microbolometer pixels exhibit sharply diminished absorption at terahertz frequencies—FPA sensitivity is significantly reduced at terahertz frequencies. Indeed, NETD of the camera has been previously calculated to be at least 3 K within the 1-5 THz band of interest.[14] To the extent that this value is more than an order of magnitude larger than the commercially-specified NETD value for passive infrared imaging, external illumination is required when using the microbolometer camera for THz imaging.
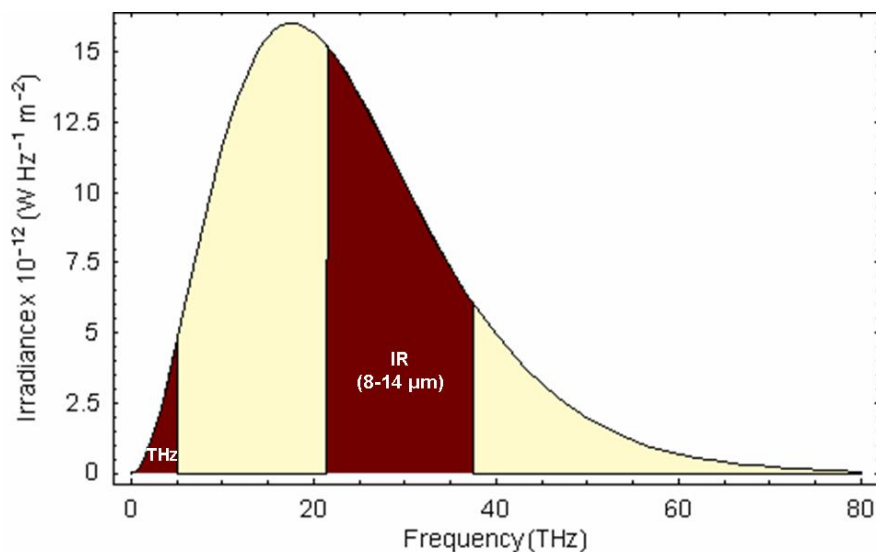
Fig. 1. Planck radiation curve for a 300 K (room temperature) blackbody, showing spectral irradiance as a function of frequency. The area of the left and right shaded regions represents total power density associated with the 1-5 THz and 21.4-37.5 THz (8-14 μm) spectral band, respectively.

2.2 QCL Source

The QCL used in these experiments, fabricated via molecular beam epitaxy (MBE) on a semi-insulating GaAs substrate, consists of a 200-μm wide and 14-μm thick multiple quantum well (MQW) active region comprised of 120 periods (Fig. 1).[16-17] To mitigate heating in the active region, the laser was nominally operated at a 300 kHz pulse repetition rate (PRF) and a duty cycle of 10-20%. With an applied current of 1.9 A, the QCL produces about 5 mW peak output power when operated below 20 K; average output power is approximately 1 mW.[17] To accommodate the laser's stringent cooling requirements, the QCL was mounted on a solid copper block (for dissipation of the thermal energy produced through ohmic heating) and operated within a closed-cycle refrigeration chamber at 10 K. Analysis of current-voltage (I-V) data indicates that dynamic impedance of the QCL during operation is approximately 2.7 Ω.

2.3 Optical Configuration

Arrangement of the complete laser assembly is as shown in Fig. 2. External to the cryostat were placed a pair of gold-plated, 90-degree off-axis parabolic reflectors (f/1 and f/2, each 50.8 mm in diameter) for focusing and steering the beam toward the camera. To minimize lateral alignment error, these reflectors were mounted upon a single optical post, and were positioned such that the highly divergent beam exiting the cold head was focused to a collimated state upon reaching the microbolometer camera. To achieve this state, the f/2 OAP was displaced 25 mm from the f/1 OAP, which was positioned 32 mm from the cryostat window. The 20-mm focal length (f/1) Tsurupica lens was mounted to the camera within a custom-designed lens assembly that replaced the original (discarded) germanium lens package mentioned previously. To properly focus the incident (collimated) beam, the lens was mounted one focal length (20 mm) from the FPA, yielding an effective camera field of view of 53°. Ideal illumination of the FPA was found to result for a camera position (as measured by the centroid of the Tsurupica lens) with 90 mm displacement from the f/2 OAP. Imaging experiments were then performed by inserting various objects roughly midway between the two parabolic mirrors, which produced a focused image at the microbolometer FPA. As suggested by the spatially close integration of components in Fig. , the total optical path length of this new configuration was kept as short as possible (within focusing constraints) to minimize beam absorption by the ambient air.
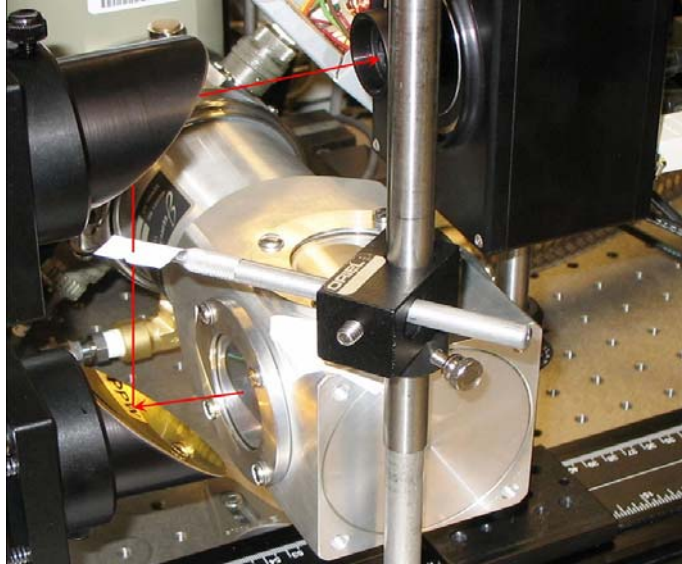
Fig. 2. Optical configuration used for terahertz imaging experiments. Lower and upper mirrors (50.8 mm and 101.6 mm focal length, respectively) are used to focus and steer the terahertz beam emerging from the Tsurupica window of the cryostat to the focal plane array of the microbolometer (beam path is illustrated by red arrow).

3. RESULTS

3.1 Beam Characterization

Fourier Transform Infrared (FTIR) analysis, performed at a resolution of 1 cm^{-1} and a mirror speed of 0.64 m/s, was used to definitively identify the resonant frequency of the QCL, and to establish the spectral lineshape associated with a typical QCL beam. As seen in Fig. 3, the full-width, half-maximum (FWHM) spectral width of the QCL beam is approximately 45 GHz, with resonance occurring at 3.57 THz (with both values exhibiting slight sensitivity to applied duty cycle).
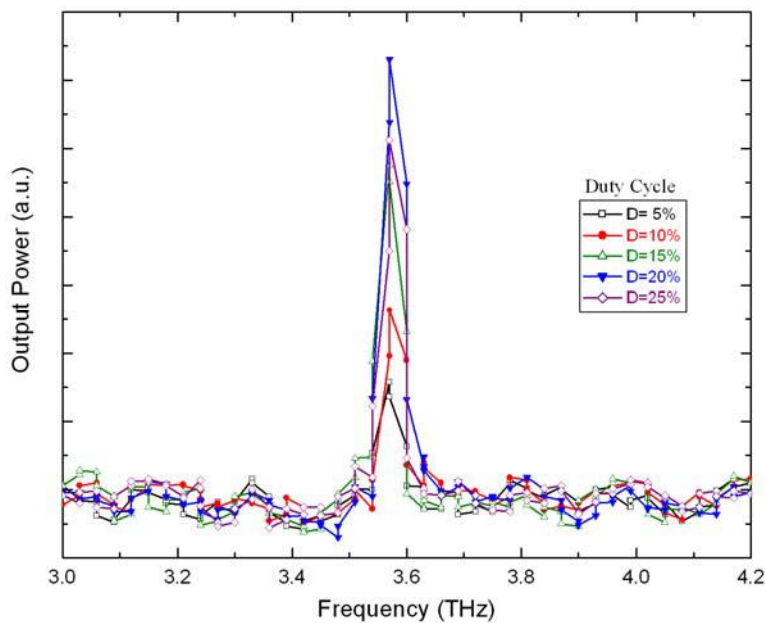

Fig. 3. Relative power detected by FTIR analysis, as a function of frequency, for various duty cycles.

FTIR analysis also provided an opportunity to further understand the relationship between duty cycle and output power over a range of applied bias currents (1.0-2.2 A). Figure 4 shows relative output power of the QCL for a range of applied currents. The laser was operated at duty cycles of 5-25% (170-830 ns pulse length) to determine the optimal pulse conditions for use in imaging experiments. Signal strength was measured by feeding the QCL beam through the external port of a Fourier transform infrared (FTIR) spectrometer and measuring the relative intensity of the resulting peak. Each FTIR measurement (consisting of 16 scans) was taken over approximately 35 seconds with an initial cryostat temperature of 10K; therefore, the results presented in Fig. 4 are only representative of the *initial* output power from the laser.
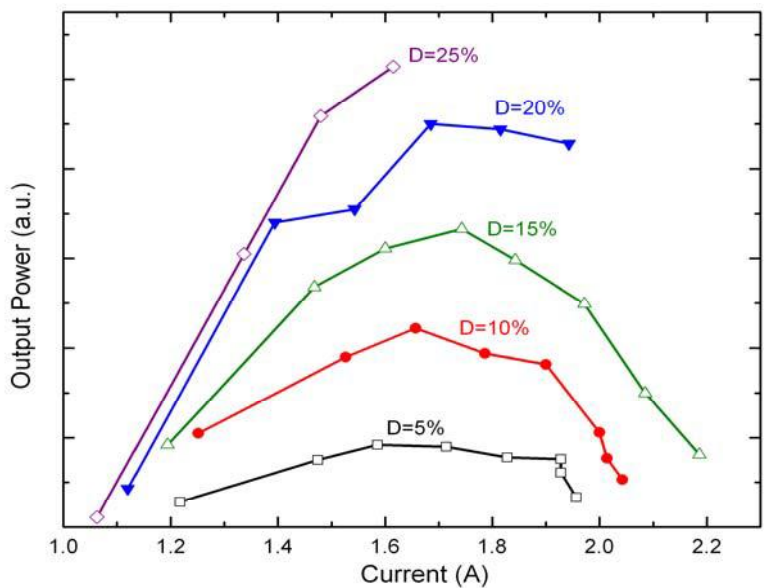

Fig. 4. Output power as a function of current for various duty cycles (D). Each data point was collected by FTIR spectrometry using 16 scans at a resolution of 1 cm^{-1} and a mirror speed of 0.64 m/s.

3.2 THz Imaging Trials

Fig. 5 is an assembly of images demonstrating the type of real-time imaging that obtainable with the optical arrangement presented above. All images were taken, using framegrabbber software, at a 30-Hz frame rate. The QCL was operated with a bias of 1.9 A at a 300 kHz pulse rate and 20% duty cycle.
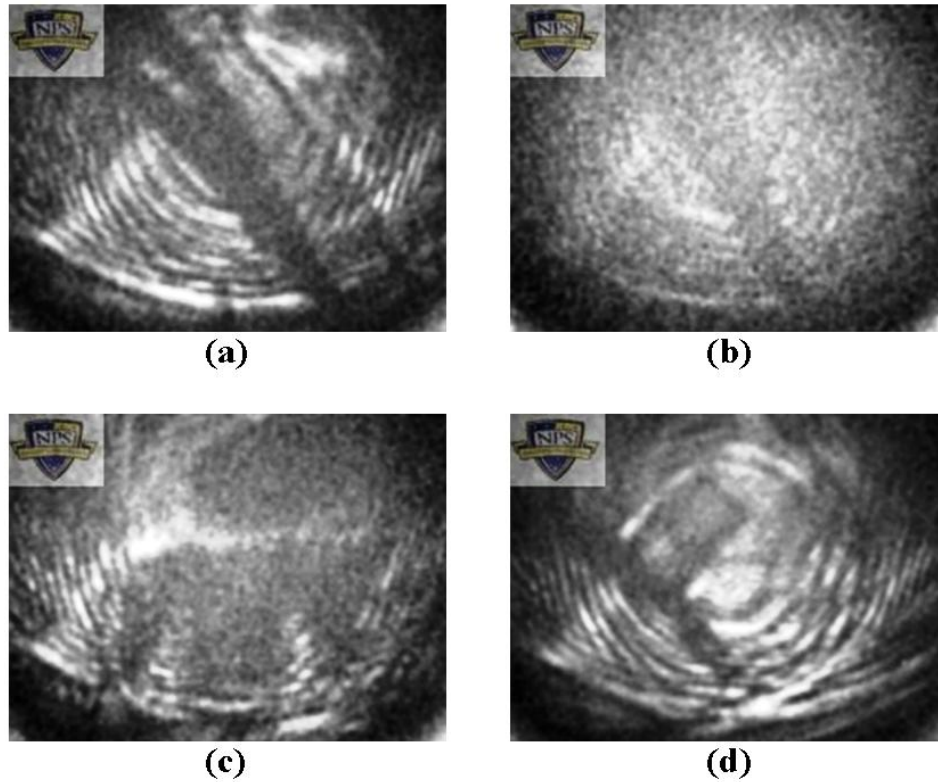

Fig. 5. Still images of video clips from imaging experiments conducted using microbolometer FPA and 3.6-THz QCL operated at a 300 kHz pulse repetition rate, 20% duty cycle, and applied bias of 1.9 A. (a) Steel utility blade obscured by two layers of opaque plastic tape. (b) Utility blade concealed with common bond paper. (c) Metalized Mylar® film cut in the shape of the Ironman Triathlon® "M-Dot" logo and enclosed by two layers of opaque plastic tape. (d) Finger of a black polyurethane glove containing an Allen wrench, which in turn is wrapped with a small swatch of opaque plastic tape.

Interest in terahertz imaging is largely driven by the fact that, whereas terahertz radiation is strongly absorbed by metals, it penetrates most non-metallic materials with little-to-no attenuation. This provides exceptional image contrast between metals and obscurants of non-metallic constitution. As is seen in Fig. 5, the contrast is particularly striking in the case of plastic obscurants. Steel blades, such as the one imaged in Fig. 5a, can be clearly seen when wrapped in opaque plastic tape—and remain visible even when enclosed by as many as eight layers of tape. To a lesser extent, metals are also detectable through cloth and common bond paper (Fig 5b). Biaxially-oriented polyethylene terephthalate (boPET) film (more commonly known by the trade name Mylar®) was found to also strongly reflect THz radiation—even when used in exceptionally thin quantities (Fig 5c). Finally, it is noteworthy that this THz imaging scheme is also capable of imaging non-metallic materials within other non-metallic materials. In Fig 5d, the THz beam is sufficiently attenuated by both polyethylene and plastic tape that each material can be clearly distinguished from the other.

Fig. 6 contains another set of four images, taken under the same illumination scheme as in Fig. 5. Herein, more challenging sets of imaging conditions were investigated—demonstrating that available power from the QCL is somewhat inadequate for penetrating thicker obscurants. However, image resolution is still sufficiently robust so as to allow identification of the various objects. Fig. 6a is the utility blade from Fig. 5a concealed behind a single layer of

relatively thick (2 mm) Plexiglas. Fig. 6b demonstrates the strong terahertz attenuation associated with even thin layers of sponge-like foam packing material. In this image, an embedded 0.5-mm lead from a mechanical pencil is barely resolvable. Fig. 6c is extended video recording of terahertz imaging of a U.S. $5 bill. Notable in this image are two types of government security (anti-counterfeit) features: a vertically-oriented narrow plastic thread (~ 1 mm in width) and an internal watermark of President Abraham Lincoln (3 mm long by 2 mm wide) on the left and right extremes of the bill, respectively. (Neither security feature is visible under normal observation; however, each can be detected when back-illuminated by a white light source.)
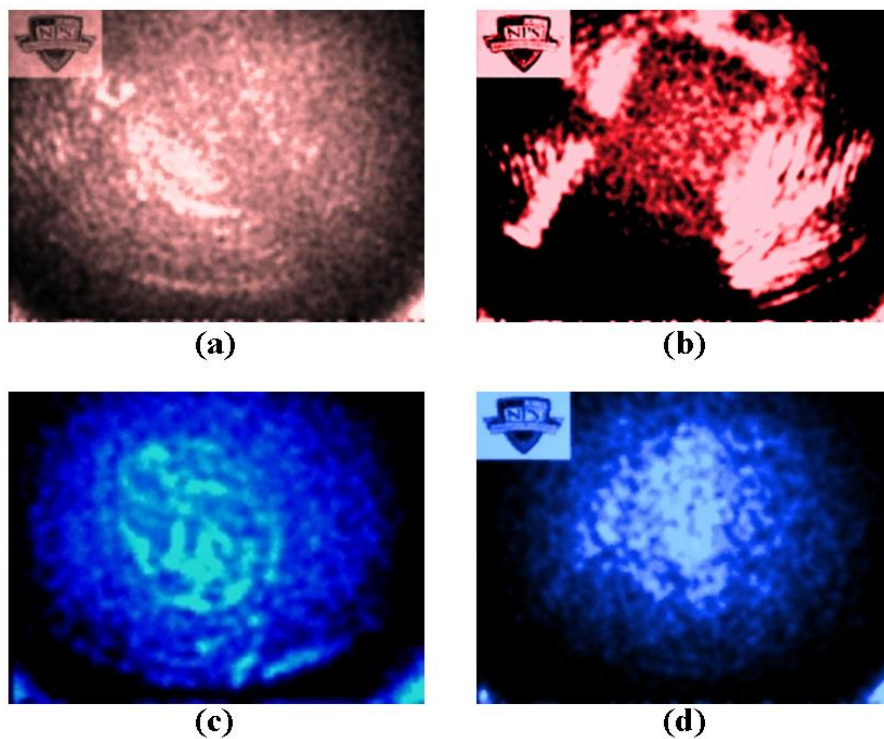

Fig. 6. Single frame captures of video recordings (with colorizing and post-processing filters applied) from imaging experiments conducted using microbolometer FPA and 3.6-THz QCL operated at a 300 kHz pulse repetition rate, 20% duty cycle, and applied bias of 1.9 A. (a) Steel utility blade obscured by a layer of Plexiglas. (b) mechanical pencil lead embedded in foam. (c) Watermark of President Abraham Lincoln from a U.S. $5 bill (embedded video clip also includes imaging of plastic security thread). (d) "NPS" ("N" in still-frame image) written in number-two pencil, on a sheet of common bond paper.

Great Britain Pound (GBP) notes arguably contain some of the most robust security features of any currency in the world. For this (and other) reasons, it is also a superb choice for examination under terahertz imaging. For purposes of this research, a £5 note was used as the imaging specimen. As with U.S. currency notes, British notes contain a watermark which (when using a conventional white light source) is only visible under back-illumination (Fig 7a). As seen in Fig. 7b, this watermark is clearly discernable in terahertz images as well. While the terahertz image does not contain the same level of detail and clarity produced by rear-illumination of visible light, it does potentially provide an additional layer of security against counterfeit practices by making watermark duplication more difficult (insofar as any attempt at watermark forgery would need to be visible under both imaging schemes).
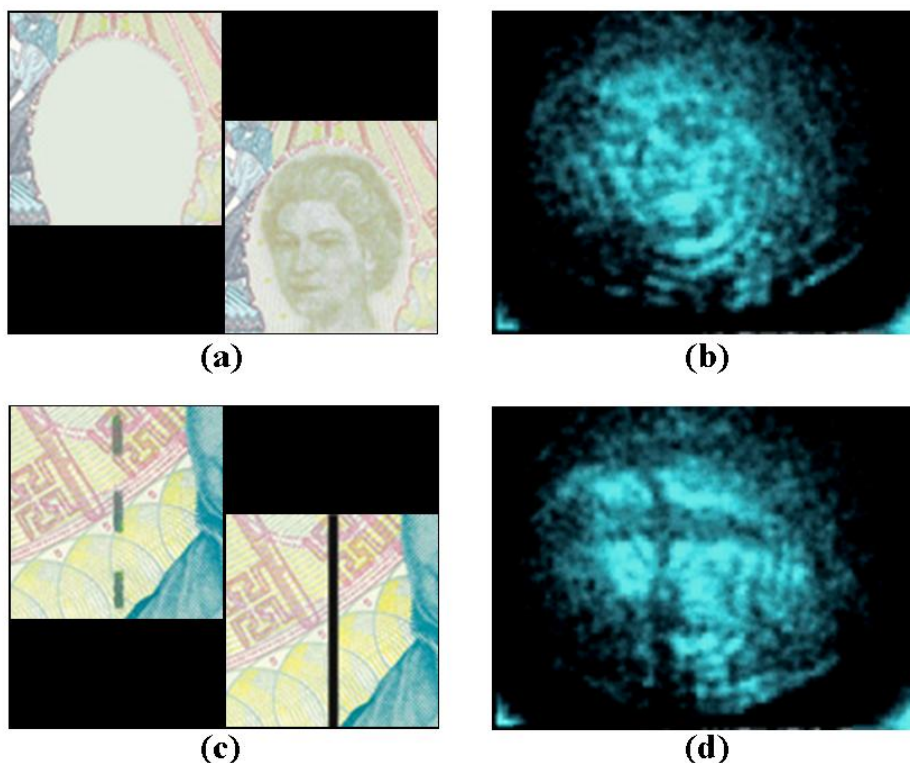
Fig. 7. £5 Great Britain Pound (GBP) note. (a) Watermark image of Queen Elizabeth II, as seen under illumination by forward-incident and rear-incident white light source (top-left and bottom-right corners, respectively). Only under the latter scheme is the watermark visible. (b) Real-time terahertz imaging of watermark using microbolometer FPA and 3.6-THz QCL operated at a 300 kHz pulse repetition rate, 20% duty cycle, and applied bias of 1.9 A (with post-processing filters applied). (c) £5 security thread as seen under illumination by forward-incident and rear-incident white light source (top-left and bottom-right corners, respectively). (d) Terahertz image of security thread (using same operating parameters as in (b)). Notable in this animation is the elaborate *cross*-thread structure, a security feature which is completely undetectable using white light sources.

More impressive is the ability of terahertz imaging to detect GBP security features which tend to elude normal visual inspections. British notes contain an internal security thread which is decidedly more complex than those found within U.S. currencies. The thread (Fig 7b), which appears as a dashed and solid line when viewed under illumination by forward-incident and rear-incident white light sources, respectively, also contains an elaborate cross-thread structure which is not immediately visible under white light illumination. As seen in Fig 7d, terahertz imaging reveals that these cross-threads, which are remarkably elongated in the lateral dimension, appear at regular intervals along the entire length of the security thread. (The strong attenuation of terahertz radiation by these cross-stitches suggests that they are quite likely metallic in nature.) Given the fact that these imaging results are produced using a rather weak illumination beam (roughly 1 mW), the feasibility of using microbolometers for THz imaging is indeed promising. With a laser source capable of higher power levels, still better image quality should be achievable—allowing for imaging through even thicker layers of non-metallic materials.

4. SUMMARY

In an attempt to further demonstrate the potential utility of terahertz imaging for homeland security applications, the authors have investigated the feasibility of imaging both metallic and nonmetallic objects with a microbolometer-based FPA camera using relatively low (milliwatt-scale) power from a terahertz-band QCL. While the ability of terahertz radiation to detect and identify metal objects has been well-established, the suitability of this spectral band to image various nonmetallic materials—especially at low illumination powers—has been much less understood. The results presented here confirm that terahertz imaging is potentially suitable for a broad variety of imaging applications, to include detection of various metallic and nonmetallic materials, concealed writing, watermark detection, and sophisticated security countermeasures used in US and foreign government currency notes. Real-time, extended imaging video files corresponding to each of the still figures in this paper are available upon request. Inquiries for such multimedia should be addressed to the corresponding author at bnbehnke@nps.edu.

ACKNOWLEDGEMENTS

REFERENCES

1. M. B. Campbell and E. J. Heilweil, "Noninvasive detection of weapons of mass destruction using THz radiation," Proc. SPIE 5070, 38 (2003).
2. M. J. Fitch, D. Schauki, C. A. Kelly, and R. Osiander, "Terahertz imaging and spectroscopy for landmine detection," Proc. SPIE 5354, 45 (2004).
3. J. F. Federici, D. Gary, R. Barat, and D. Zimdars, "THz standoff detection and imaging of explosives and weapons," Proc. SPIE 5781, 75-84 (2005).
4. D. A. Zimdars and J. S. White, "Terahertz reflection imaging for package and personnel inspection," Proc. SPIE 5411, 78 (2004).
5. T. Globus, D. Theodorescu, H. Frierson, T. Kchromova, and D. Woolard, "Terahertz spectroscopic characterization of cancer cells," Progress in Biomedical Optics and Imaging 6, 233-240 (2005).
6. R. H. Clothier and N. Bourne, "Effects of THz exposure on human primary keratinocyte differentiation and viability," J. Biol. Phys. 29, 179–85 (2003).
7. J. E. Bjarnason, T. L. J. Chan, A. W. M. Lee, M. A. Celis, and E. R. Brown, "Millimeter-wave, terahertz, and midinfrared transmission through common clothing," Appl. Phys. Lett. 85, 519 (2004).
8. P. Y. Han and X. C. Zhang, "Free-space coherent broadband terahertz time-domain spectroscopy," Meas. Sci. Technol. 12, 1747–1756 (2001).
9. Y. Watanabe, K. Kawase and T. Ikari, "Component spatial pattern analysis of chemicals using terahertz spectral imaging," Appl. Phys. Lett. 83, 800 (2003).
10. G. Karunasiri, "Real time THz camera using microbolometer focal plane array," 7th Int. Conf. on Technol. & the Mine Problem, May 2-4, (2006), Monterey, CA.
11. A. W. M. Lee, and Q. Hu, "Real-time, continuous-wave terahertz imaging by use of a microbolometer focal-plane array," Optics Lett. 30, 2563 (2005).
12. A. W. M. Lee, B. S. Williams, Q. Hu, and J. L. Reno, "Real-time imaging using a 4.3-THz quantum cascade laser and a 320x240 microbolometer focal-plane array," IEEE Photon. Tech. Lett. 18, 1415 (2006).

13. B. N. Behnken, M. Lowe, G. Karunasiri, D. Chamberlin, P. R. Robrish, J. Faist, "Detection of 3.4 THz radiation from a quantum cascade laser using a microbolometer infrared camera," Proc. SPIE 6549, 65490C (2007).

14. B. N. Behnken, G. Karunasiri, D. R. Chamberlin, P. R. Robrish, and J. Faist, "Real-Time Imaging Using a 2.8 THz Quantum Cascade Laser and Uncooled Infrared Microbolometer Camera," Opt. Lett. 33, 440-442 (2008).

15. R. A. Wood, "Monolithic silicon microbolometer arrays," in Semiconductors and Semimetals 47, 43-121 (1997).

16. J. Faist, L. Ajili, G. Scalari, M., Giovannini, M. Beck, M. Rochat, H. Beere, A.G. Davies, E.H. Linfield & D. Ritchie, "Terahertz quantum cascade lasers," Phil. Trans. R. Soc. Lond. 362, 215-231 (2003).

17. D. R. Chamberlin, P. R. Robrish, W. R. Trutna, G. Scalari, M. Giovannini, L. Ajili, and J. Faist, "Imaging at 3.4 THz with a quantum-cascade laser," Appl. Opt. 44, 121-125 (2005).